

*Supplementary Information*

**Long-lived and Well-resolved  
Mn<sup>2+</sup> Ion Emissions in CuInS-ZnS Quantum Dots**

*Sheng Cao<sup>1,2</sup>, Chengming Li<sup>1</sup>, Lin Wang<sup>2</sup>, Minghui Shang<sup>2</sup>, Guodong Wei<sup>2</sup>, Jinju Zheng<sup>2,\*</sup>,  
and Weiyou Yang<sup>2,\*</sup>*

<sup>1</sup> School of Materials Science and Engineering, University of Science and Technology Beijing, Beijing  
100083, China.

<sup>2</sup> Institute of Materials, Ningbo University of Technology, Ningbo 315016, China.

\* **Corresponding Authors, E-mails:** zhengzhao2007@163.com (J. Zheng) and  
weiyouyang@tsinghua.org.cn (W. Yang)  
**Tel:** +86-574-87080966  
**Fax:** +86-574-87081221

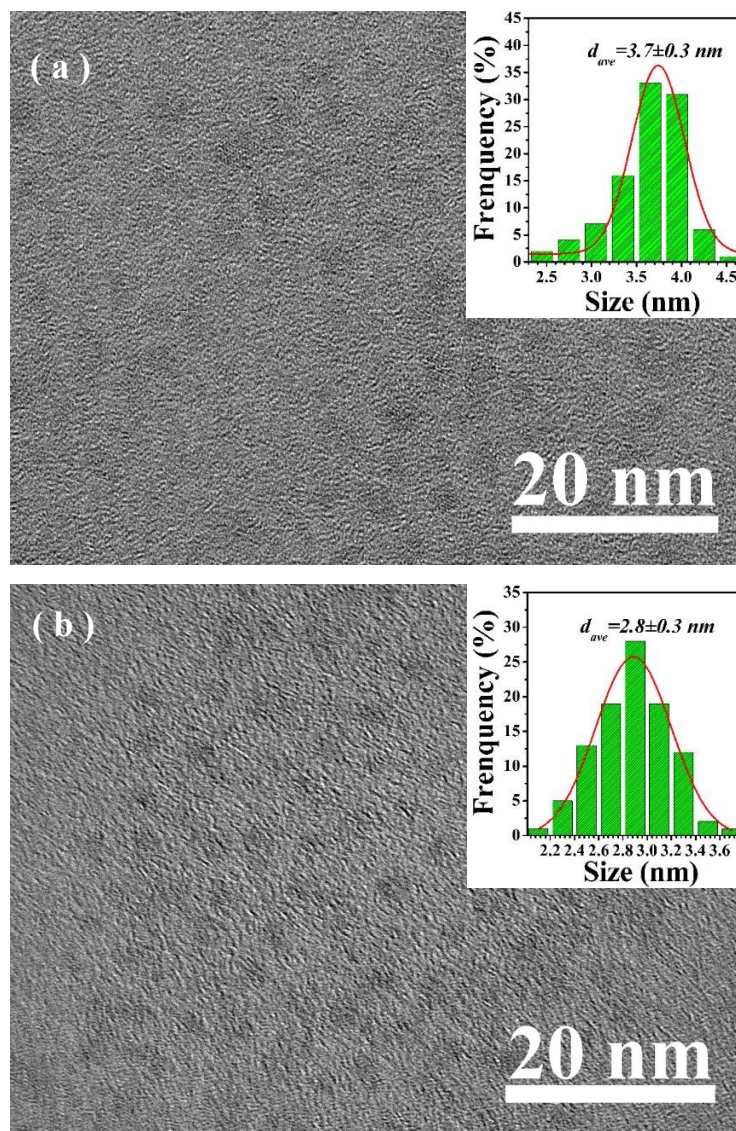


**Figure S1** Typical TEM images and the corresponding size distributions (insets) of the Mn<sup>2+</sup>-doped CIS-ZnS QDs (a) and CIS cores coated with a Zn<sub>1-x</sub>Mn<sub>x</sub>S shells obtained after the second step in the hot-injection method (b). It should be pointed out that the pure CIS cores obtained after the first step in the hot-injection method are too small to be clearly detected by TEM.

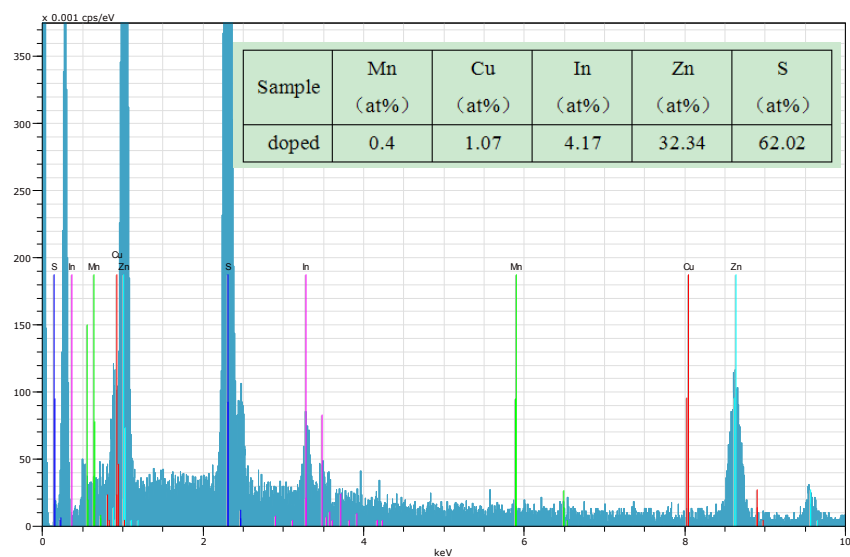


**Figure S2** Typical EDX spectrum of  $\text{Mn}^{2+}$ -doped CIS-ZnS QDs. The inset shows the detailed chemical compositions.

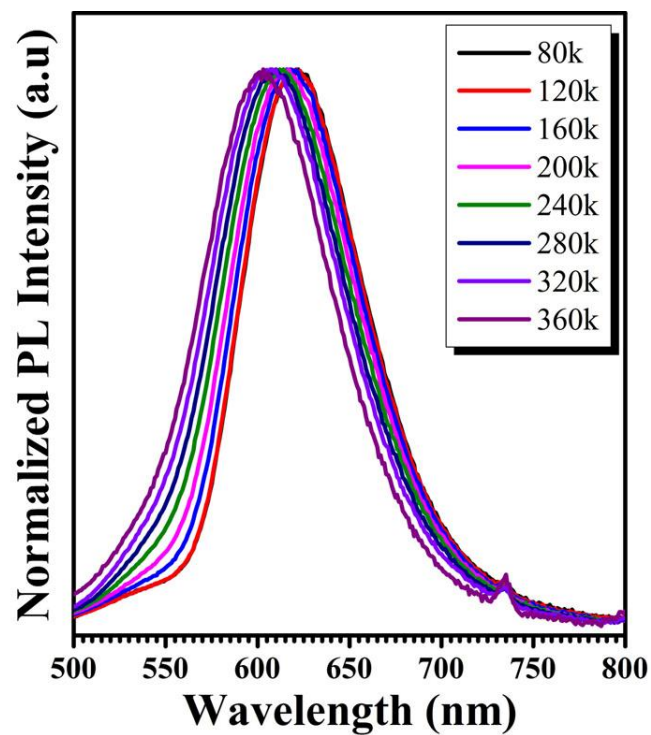


**Figure S3** The normalized temperature-dependent PL spectra of  $\text{Mn}^{2+}$ -doped CIS-ZnS QDs recorded in the range from 80 to 360 K. The PL peaks are blue shifted systematically with the increase of temperatures, which is consistent with a typical emission of  $\text{Mn}^{2+}$  ion in II-VI semiconductor QDs due to its *d-d* transition



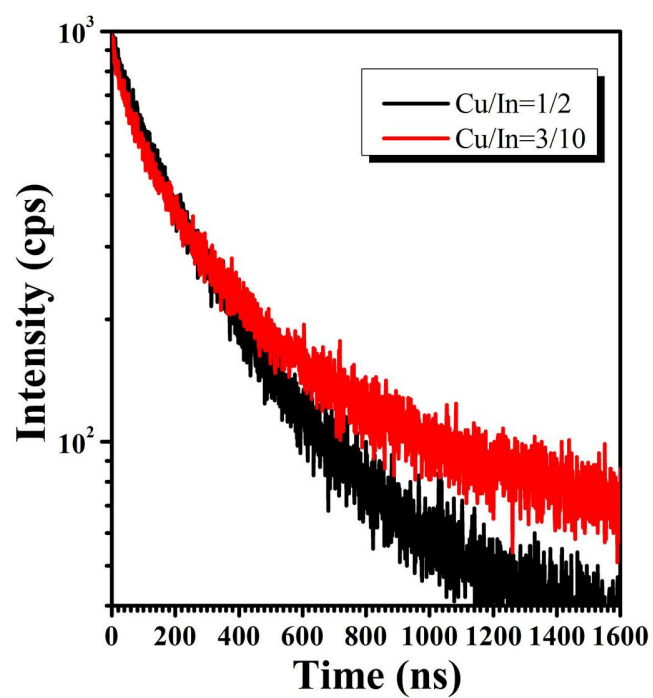


**Figure S5** Typical decay curves of the  $\text{Mn}^{2+}$ -doped CIS-ZnS QDs at the Cu/In molar ratio of 1/2(black line) and 3/10(red line), respectively.

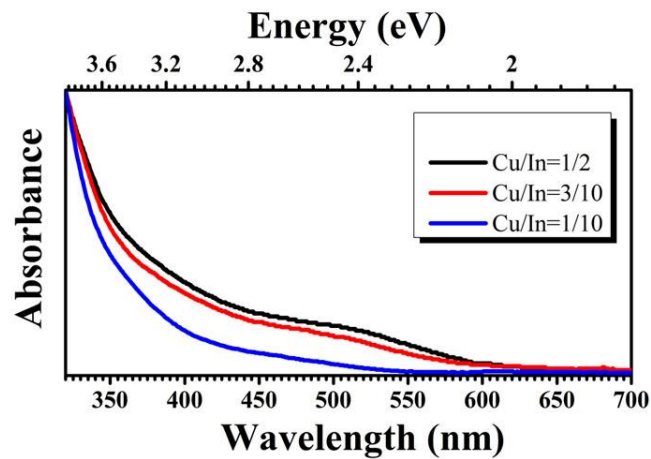


**Figure S6** The representative UV-vis absorption spectra of Mn<sup>2+</sup>-doped CIS-ZnS QDs at the Cu/In ratios of 1/2, 3/10 and 1/10, respectively. The absorption band edges show blue shifts with the decrease of the Cu/In ratios, indicating the corresponding increase of the bandgap energy.

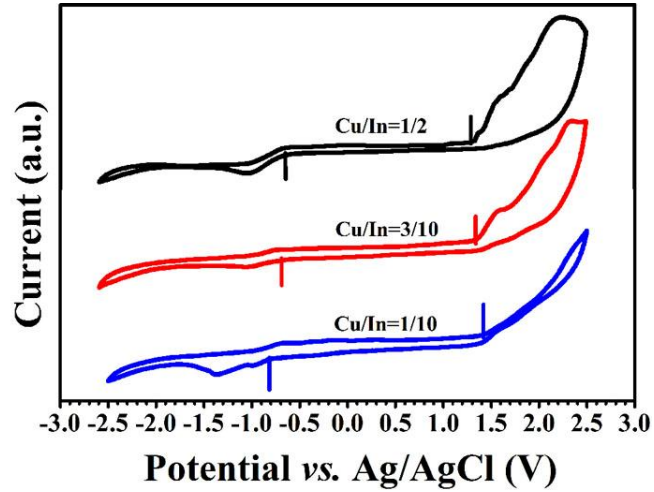


**Figure S7** Typical cyclic voltammograms of  $\text{Mn}^{2+}$ -doped CIS-ZnS QDs at the Cu/In ratios of 1/2, 3/10, 1/10, respectively. These experimental results imply that, with the decrease of Cu/In ratios, the absolute value of the onset oxidation potential ( $E_{ox}$ ) and reduction potential ( $E_{red}$ ) become larger, which indicates the increase of the bandgap energy, and consistent with the UV-vis absorption spectra.



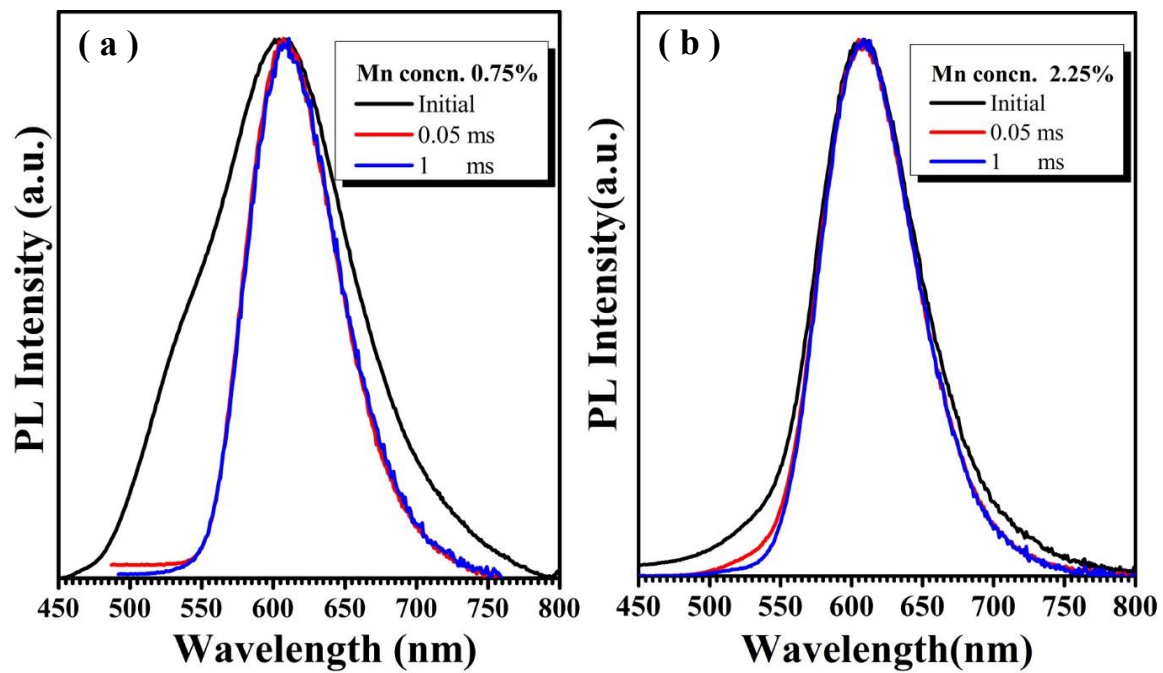


**Figure S8** Normalized time-resolved PL spectra of  $\text{Mn}^{2+}$ -doped CIS-ZnS QDs with the nominal  $\text{Mn}^{2+}$  concentrations of 0.75% and 2.25%. The delay times are 0.05 ms (red lines) and 1 ms (blue lines), respectively, as compared to the initial emission.

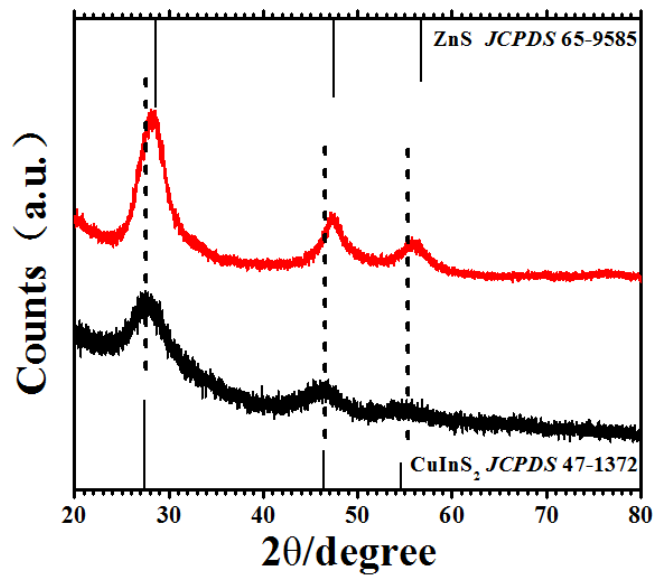


**Figure S9** XRD patterns of the CIS cores coated with a Zn<sub>1-x</sub>Mn<sub>x</sub>S shells (black) obtained after the second step in the hot-injection method and Mn<sup>2+</sup>-doped CIS-ZnS QDs (red).

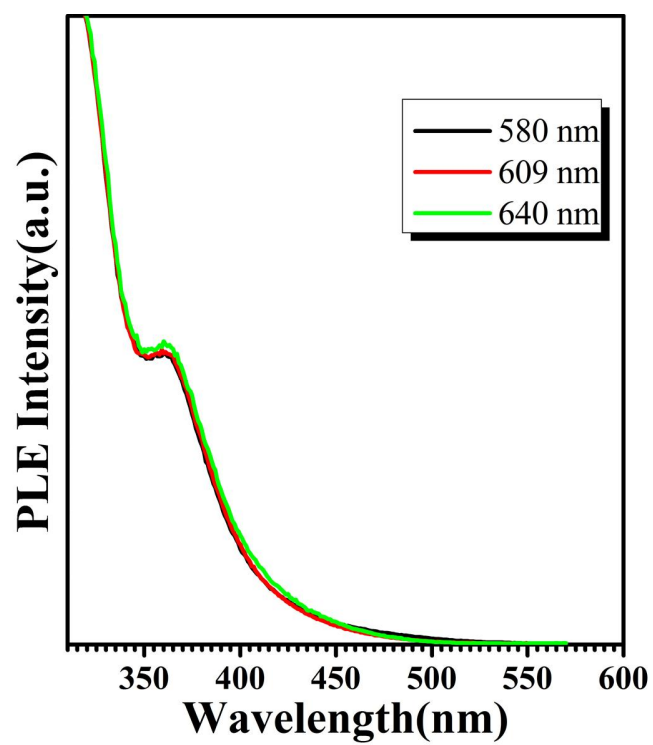


**Figure S10** Normalized PLE spectra of Mn<sup>2+</sup>-doped CuInS-ZnS QDs detected at different emission wavelengths, disclosing the homogeneous local environments of the emission centers.